Mansoura Engineering Journal

Volume 40 | Issue 1 Article 7

7-5-2020

Numerical Simulation of a White Blood Cell Motion within an Arteriole.

Mohamed Mansour
Mechanical Power Engineering Department, Faculty of Engineering, Mansoura University, El-Mansoura 35516, Egypt, mhsaadanym@mans.edu.eg

Numerical Simulation of a White Blood Cell Motion within an Arteriole

محاكاة عددية لحركة كرة دم بيضاء في شريان دقيق

Mohamed H. Mansour
Mechanical Power Engineering Department, Faculty of Engineering,
Mansoura University, El-Mansoura 35516, Egypt
E mail: mhsaadanym@mans.edu.eg

الخلاصة:

تمت محاكاة حركة كرة دم بيضاء في شريان دقيق عدديا باستخدام النموذج ذوالست درجات من الحريه والشبكة الديناميكيه الموجودين ضمن برنامج FLUENT. ولدراسة تأثير الخاصية الغير نيوتونية على حركة كرات الدم البيضاء، تمت معامله المائع الحاوي لكرة الدم البيضاء كمائع نيوتوني ومرة أخرى كمائع غير نيوتوني. أظهرت النتائج أن كرة الدم البيضاء تتحرك بسرعة أقل من سرعة الدم ودائما تتحرك نحو محور الشريان (بغض النظر عن وضعها المحوري). ولجعل النموذج أكثر واقعية تم الأخذ فى الاعتبار تأثير كرات الدم الحمراء على حركة كرة الدم البيضاء وذلك بإضافة معادلة جديدة للمعادلات الحاكمة للسريان (باستخدام طريقة UDF الموجوده في FLUENT) وهي معادلة السريان لكرات الدم الحمراء. إضافة تلك المعادلة أدت إلى تغيير في النتائج نتيجة القوى المتبادلة بين كرات الدم الحمراء والبيضاء، حيث وجد أن كرة الدم البيضاء تتحرك باتجاه المحور أو الجدار بناء على وضعها المحوري في حالة السريان الغير نيوتوني.

Abstract

The motion of a leukocyte (White Blood Cell) within a straight vessel, representative of an arteriole, is simulated using dynamic meshing and a six-degree-of-freedom model within FLUENT (FLUENT Inc.). The fluid is modelled as both Newtonian and non-Newtonian to simulate the bulk effects of blood. The results showed that the leukocyte lags the undisturbed velocity profile and migrates towards the centreline at all radial locations. Haematocrit is also modelled as a scalar transported by the flow and a model is introduced via a User-Defined Function (UDF) to generate a force based on the haematocrit effect. This additional forcing results in inward radial migration and outward radial migration based on the WBC radial position for the non-Newtonian case.

Keywords

Blood – Leukocyte – Haematocrit – Six-degree-of-freedom model – Radial migration.

1. Introduction

Blood is a suspension of many different particles within a fluid called plasma. The interaction between these particles results in complex flow dynamics and a non-Newtonian flow. The particles include the oxygen carrying Red Blood Cells (RBCs), disease fighting White Blood Cells (WBCs) and platelets, (Fung, 1996).

Leukocytes (WBCs) are closely linked to the body's immune system. They constitute a Newtonian cytoplasm surrounded by a membrane and are typically spherical in shape (Schmid-Schönbein, 1987 and Alexandrova & Antonova, 2012). As the flow rate decreases and the vessels become narrower both WBCs and platelets are driven towards the wall by Brownian motion. This process is known as margination and is highly important for the body's immune system as the WBCs and platelets are required at the walls of capillaries (Freund, 2007). Since WBCs are rigid spheres, the motion of a WBC in blood can be simulated as a sphere moves in a vessel.

There are many parameters which affect the motion of the particle and the most commonly investigated include the Reynolds number ($\mathrm{Re} = \frac{8a_W^2 \rho_B V_{Max}}{\mu_B a_V}$), particle to vessel radius ratio (λ) and

Received: 8 December, 2014 – Revised: 11 January, 2015 - Accepted: 11 January, 2015

particle to fluid density ratio (ρ'). In the Re number definition equation a_W, ρ_B, V_{Max}, μ_B and a_V represents the WBC radius, the blood density, the maximum axial velocity, the blood dynamic viscosity and the vessel radius, respectively. The motion of the particle is typically described by three parameters: the translational velocity (V_T), the radial migration velocity (V_r) and the non-dimensional radial position at which the particle reaches equilibrium ($\beta = R/a_V$).

Considering a neutrally buoyant sphere convicted within a Poiseuille flow, Karnis et al. (1966) demonstrated experimentally that the sphere will translate with a velocity slightly lower than the undisturbed local velocity. Thus, the translational velocity exhibits a parabolic profile similar to the Poiseuille profile, with the peak at the centreline and the lowest velocity near the wall. This result has been confirmed both numerically and experimentally by Feng et al. (1994) and Feng & Michaelidis (2002) using a finite element method. The difference between the undisturbed local velocity and the particle velocity is known as the slip velocity (u_S) and has been shown to depend on ρ'. Yu et al. (2004) demonstrated that dense particles lag the fluid to a greater extent resulting in a larger slip velocity, whilst lighter particles actually lead the flow, giving negative slip velocities.

By the symmetry of the velocity profile, it can be seen that the centreline will be an equilibrium position in a radial sense. However, Feng et al. (1994) explain that it is an unstable one as once the particle moves away from the centreline and it will not return. The curvature of the velocity profile results in a rotation of the sphere as if it was rolling along the closest wall resulting in a Magnus type lift force directed towards the wall and radial migration (Matas et al., 2004).

Segré & Silberberg (1961) carried out a comprehensive set of experiments at low Reynolds numbers which demonstrated that a sphere will migrate away from both the centreline and the wall to an equilibrium position of roughly β = 0.63. Also, Karnis et al. (1966), Cox & Mason (1971) and Matas et al. (2004) calculated experimentally the non-dimensional radial position at which the particle reaches equilibrium. While, the numerical investigations conducted by Feng et al (1994), Yu et al. (2004), Yang et al. (2005), Pan & Glowinski (2005) and Pozrikidis (2005) found that as the particle size increases or the Reynolds number decreases, the equilibrium position moves closer to the centre. The β values ranged from 0 to 0.85 for both experimental and numerical investigations.

Furthermore, collisions of WBCs with RBCs lead to discrete changes in the particles radial position. Freund (2007) studied the particle histories to highlight the stochastic behaviour of the WBC in the existence of RBCs. He concluded that the WBC equilibrium position was near the edge of the RBC cell-free-layer. Collisions with RBCs lead to discrete changes in the particles radial position and this clearly demonstrates the importance of modelling individual particles. Also, Fedosov et al. (2012) concluded that the RBC aggregation increases the WBC margination rate. Mahdi et al. (2014) studied experimentally the motion of leukocyte in a venue. They could not calculate the forces acting on the leukocyte in all the directions.

Based on the previous review, the aim of the present paper is to create a realistic numerical model which is capable to simulate the dynamic motion of a leukocyte or white blood cell through an arteriole. The WBC motion is based on the forces and torques it experiences as it is convicted by the fluid. Then, the non-Newtonian behaviour of the carrying fluid is examined to study its effect on the WBC motion. Finally, the effects of erythrocyte or red blood cell (RBC) concentration (haematocrit) on WBC margination are presented.

2. Mathematical model

2.1. Governing equations

The mass and momentum conservation equations for an incompressible flow can be written as

$$\frac{\partial \rho}{\partial t} + \nabla . \left(\rho \vec{V} \right) = 0 \qquad (1)$$

$$\frac{\partial \left(\rho \vec{V} \right)}{\partial t} + \nabla . \left(\rho \vec{V} \vec{V} \right) = -\nabla p + \nabla . \left[\mu \left(\nabla \vec{V} + \vec{V}^{T} \right) \right] + \rho \vec{g} + \vec{S} \qquad (2)$$

where ρ, μ, $\vec{V}$, p and $\vec{S}$ denote the density, the viscosity, the velocity field, the pressure and the source term.

Within the FLUENT software, the moments, pressure forces and shear forces are calculated and integrated along with the WBC automatically when the six-degree-of-freedom (SDOF) model is selected. Then, the translational and angular velocities of the centre of gravity of the WBC can be computed using the following equations (Fluent Inc.);

$$\vec{V}_T = \frac{1}{m} \sum \vec{f}_G \qquad (3)$$

$$\dot{\vec{\omega}}_W = L^{-1} \left(\sum \vec{M}_W - \vec{\omega}_W \times L \vec{\omega}_W \right) \qquad (4)$$

where $\vec{V}_T$, m and $\vec{f}_G$ are the WBC translational motion, the WBC mass, and the force vector due to gravity, respectively. While $\dot{\vec{\omega}}_W$, L, $\vec{M}_W$ and $\vec{\omega}_W$ are the angular motion, the inertia tensor, the WBC moment vector and the WBC angular velocity vector, respectively. After the computation of translational and angular motions, the new WBC coordinates and position can be determined by using the dynamic mesh technique which is implemented in FLUENT software.

The distribution of Haematocrit, *H*, throughout the vessel can be modelled as a scalar. This scalar is convected with the flow based on the following transport equation (Bressloff et al., 2009).

$$\frac{\partial \rho H}{\partial t} + \nabla . \left(\rho \vec{V} H - \Gamma \nabla H \right) = 0 \qquad (5)$$

where $\vec{V}$ and Γ are the convective velocity and the diffusion coefficient, respectively.

3. Numerical approach

The problem is simulated numerically using FLUENT 6.3.26 software (ANSYS Inc.). A user-defined-function (UDF) of SDOF model is introduced to simulate the motion of the sphere. Also, a user-defined-scalar (UDS) is used to add a new haematocrit conservation equation. The only model constant in Eq. (5) that needs to be defined is the diffusion coefficient (Γ). This constant defines how quickly the haematocrit diffuses through the flow and has a large impact on the overall haematocrit profile. A constant Γ value of 1e-8 is taken to ensure that the haematocrit profile at the location of the WBC is representative of a real blood flow (Bressloff et al., 2009). The option for a non-Newtonian power law fluid is built into FLUENT. The value of the consistency index (K), power index (n), viscosity at zero shear rate and viscosity at infinite shear rate (non-Newtonian model parameters) are 0.017 Pa^n, 0.708, 0.0035 Pa.s and 0.056 Pa.s, respectively, (Shibeshi & Collins 2003).

3.1 Geometry and Grid

A straight vessel of constant circular cross-section is used to represent an arteriole, with the WBC modelled as a rigid sphere of constant density. Both Newtonian and non-Newtonian fluids are considered as a carrying fluid that is representative of blood. Typical parameters for flow in an arteriole are given in Table 1.

Parameter	Value
Vessel / arteriole radius, a_V	25 □m
Arteriole length, l	100 μm
WBC radius, a_W	5 □m
a_V / a_W	5
WBC density, ρ_W	1070 kgm^{-3}
Blood density, ρ_B	1061.5 kgm^{-3}
Blood dynamic viscosity, μ_B	0.00345 Pa.s
Blood mean velocity, V_M	0.00375 ms^{-1}
Re	0.0185

Table 1. Typical parameters for flow in an arteriole (Freund, 2007)

The geometry and mesh were generated in GAMBIT software (ANSYS Inc.) using tetrahedral elements. A cylinder with the origin located at the center of one face, is extruded to form a solid rod. The representation of the white blood cell is introduced by cutting out a spherical hole.
Four homogenous meshes (A-D) were applied to the unsteady case, where the WBC is allowed to move freely. The meshes A, B, C and D have roughly 12,000, 63,000, 163,000 and 1,136,000 cells respectively. There was a relatively small variation between the results for meshes C and D. This suggests that mesh C is quite accurate enough to be used in the next simulations.

3.2 Boundary Conditions

The boundary conditions are taken as a constant pressure of 585.66 kPa at the inlet to obtain a realistic value of the blood velocity in an arteriole as given in Table 1 and an atmospheric pressure at the outlet. The no slip boundary is applied to the vessel wall and the WBC surface. The haematocrit value at the wall and inlet are taken as zero and 0.45, respectively, whilst the outlet and WBC are set as zero flux.

4. Results and discussion

The motion of a WBC in a microvessel was investigated numerically in both steady and unsteady states. Furthermore, the flows of the WBC in Newtonian and non-Newtonian liquids were studied to understand the effect of changing fluid properties on the motion and trajectory of the WBC.

4.1 Steady State Flow Patterns and Forces

Figure (1) illustrates the streamlines around a WBC. It is indicated that the flow is highly viscous as it remains attached around the sphere and there is no wake. Furthermore, the influence of the sphere quickly dissipates, showing that the results will not be affected by the domain length.
The forces acting on the sphere in axial and radial directions at different radial locations are drawn against the dimensionless radial position (r) in Figs. (2&3), respectively. In each of these figures, the force has been normalized by dividing it by the dynamic pressure based on the mean velocity.

$$C_D = \frac{2f}{\rho V_M{}^2} \qquad (6)$$

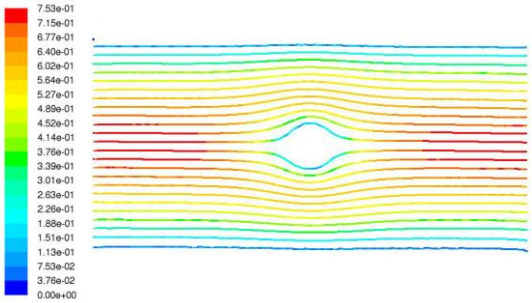

Fig. (1). Streamlines coloured by velocity magnitude on the xz-plane

It is obvious that the axial drag force is the dominant force on the WBC and causes the axial translation. The axial force demonstrates a roughly parabolic profile, similar to the Poiseuille profile. This suggests that the WBC will translate with a higher velocity when at the centreline than when closer to the wall. Also, the axial force values on a sphere moves in a Newtonian liquid is much higher than that moves in a non-Newtonian liquid at the same conditions and these differences decrease when the particle moves closer to the wall.

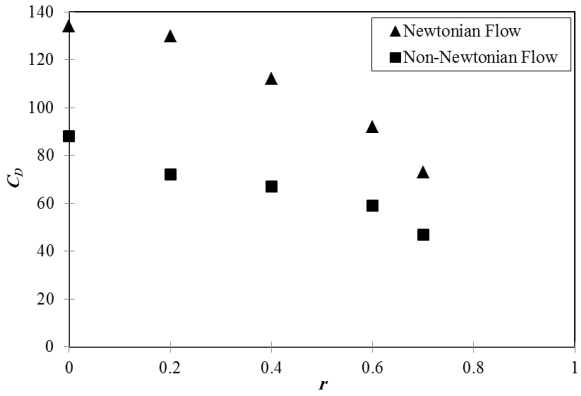

Fig. (2). Axial drag coefficient on WBC at different radial locations

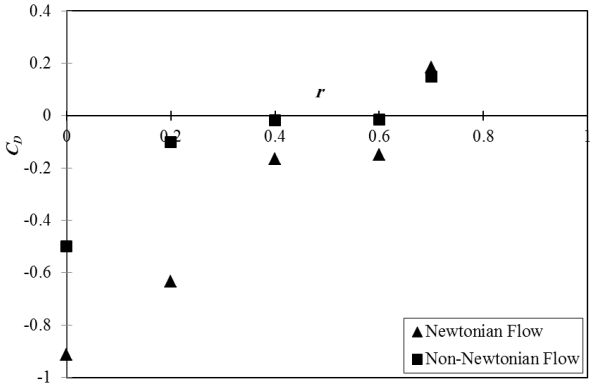

Fig. (3). Radial drag coefficient on WBC at different radial locations

On the other side, the radial force on the WBC exhibits a roughly linear variation with radial location as shown in Fig. (3). It is found that the dimensionless equilibrium position (β) occurs between 0.4 - 0.6 which agrees with the findings of Feng et al. (1994) ($0.45 < \beta < 0.6$) and Yang et al. (2005) ($0.57 < \beta < 0.7$). This suggests that the WBC should move away from both the centreline and the wall. Also, the radial force amplitude is higher in the Newtonian case than the non-Newtonian case.

4.2 Dynamic Flow Patterns

Initially, the WBC is released at the centre of the vessel and has little impact on the flow, which remains close to a Poiseuille profile for both Newtonian and non-Newtonian flows. The non-Newtonian power law fluid exhibits a velocity profile which is slightly blunter than the Poiseuille profile whilst the opposite can be seen for the Newtonian fluid as shown in Fig. (4).

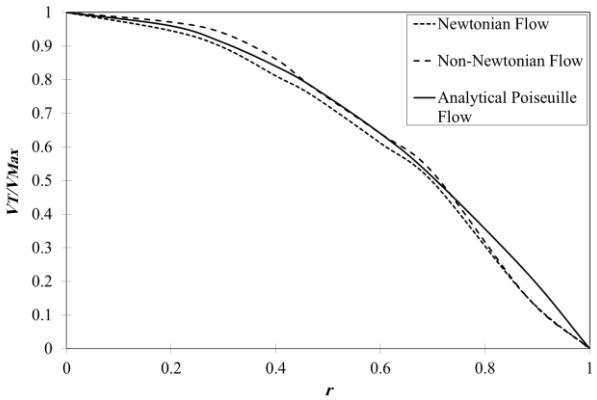

Fig. (4). Axial fluid velocity profiles at the inlet

Figure (5) illustrates the velocity contours for the non-Newtonian case at different initial radial positions ($r = 0.0,\ 0.5,\ 0.78$). It is found that the WBC has a reduced impact on the flow in comparison to the steady state solution as it is now being convected by the fluid. However, as the WBC exists closer to the wall, the effect on the flow becomes more pronounced.

4.3 Axial & Slip Velocity of WBC

Figure (6) shows the WBC translational (axial) velocity along with the fluid velocity distribution in both Newtonian and non-Newtonian cases. The axial velocity of the particles was seen to lag the fluid velocity slightly which agrees enough with the results of Feng et al. (1994) and Feng & Michaelidis (2002). The slip velocity appears to increase with the radial location. Also, the WBC slip velocity increases when it flows in a non-Newtonian liquid.

The translational velocity profile correlates well with the axial force component shown in Fig. (2). The axial force decreases with radial position and results in a lower translational velocity. Both the axial force and axial velocity component are linked to the parabolic fluid velocity profile.

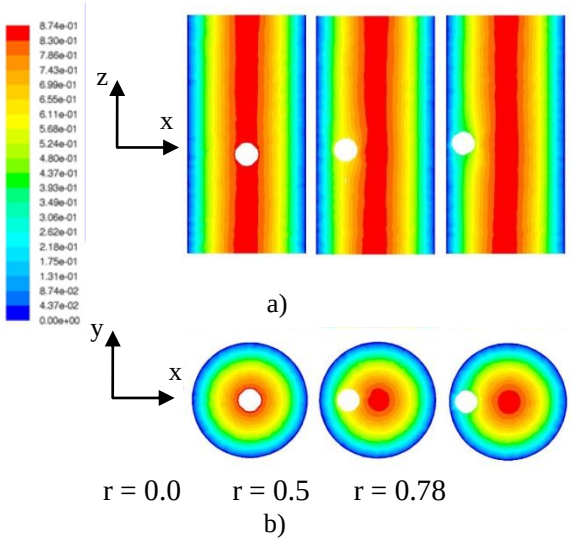

Fig. (5). Velocity contours for the non-Newtonian case on a) xz-plane at the vessel axis and b) xy-plane at the WBC centre for different initial radial positions

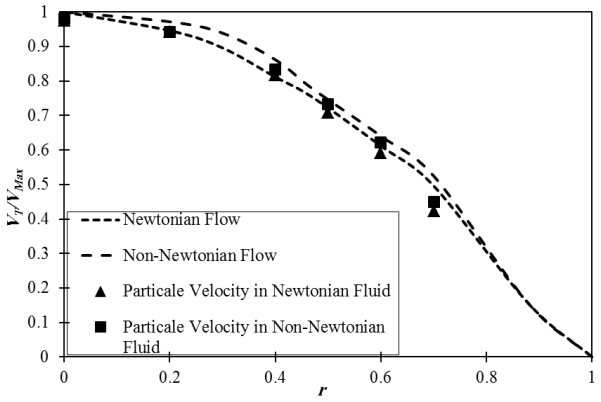

Fig. (6). A WBC translational velocity at different radial locations

4.4 Radial Migration

The WBC moves in the radial direction as well as the axial one. The radial velocity is much smaller in magnitude than the translational velocity. The comparison between Figs. (6&7) shows that a displaced sphere from the vessel centreline in the x-direction migrates back towards the centreline with a velocity approximately three to four orders of magnitude lower than the axial velocity.

As the radial velocities are relatively low, it is not possible within the current time constraints to demonstrate a WBC moving from the wall to the centreline or vice-versa. Only the radial velocities at different radial locations can be extracted and used to produce a profile across the vessel, (Freund, 2007).

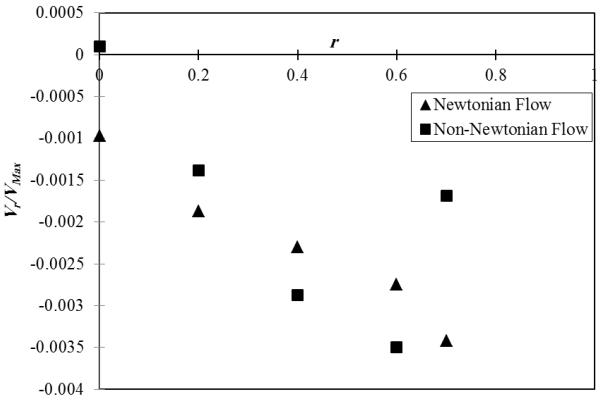

Fig. (7). A WBC radial velocity at different radial locations

Figure (7) depicts the WBC radial velocities against the radial locations. The WBC migrates towards the centre of the vessel in all radial positions. The radial velocity increases at larger radial displacements. There is no equilibrium in the radial position for the WBC flows in the Newtonian liquid. On the other hand, the non-Newtonian fluid induces a radial equilibrium position at the centreline.

4.5 Prediction of WBC Trajectories

Based on Figs. (6&7), it is possible now to generate relations to describe the translational and radial velocity variations as a function of the radial distance. The relations for the WBC which moves in a Newtonian liquid can be written as;

$$V_T(r)/V_{Max} = \left(1 - r^{1.8}\right) \qquad (7)$$

$$V_r(r)/V_{Max} = 0.0032r + 0.0011 \qquad (8)$$

and for the WBC moving in the non-Newtonian liquid, the relations become;

$$V_T(r)/V_{Max} = \left(1 - r^{2.2}\right) \qquad (9)$$

$$V_r(r)/V_{Max} = 0.0061r \qquad (10)$$

It is noted that these relations of the translational and radial velocities can provide a useful technique to predict the WBC velocity trajectory.

Figure (8) illustrates the WBC trajectory as it migrates downstream the vessel in a non-Newtonian liquid. This is achieved by using the above concluded relations to calculate the WBC velocity at any given location and then iterate through time.

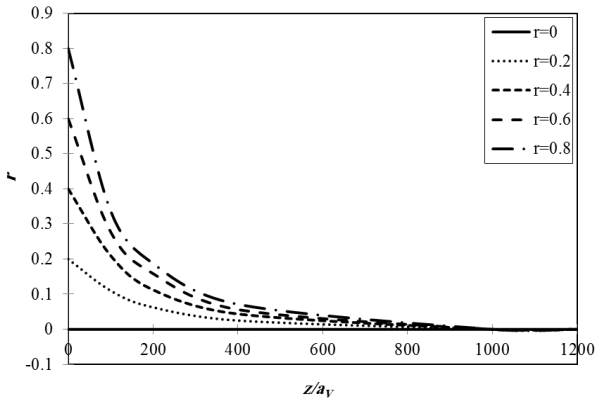

Fig. (8). Estimated particle trajectories for WBCs released at different radial locations (non-Newtonian fluid)

The estimated trajectories show that the WBCs will migrate towards the centreline of the channel. Also, the WBC translates in the axial direction 1,000 times the vessel diameter to migrate towards the centreline.

4.6 Haematocrit-Leukocyte Interaction

The model is modified to take into account the effect of haematocrit distribution on the WBC motion. The haematocrit distribution in arterioles and microvessels are characterized by the existence of cell-free layer near the wall. A constant Γ value of 1e-8 in the haematocrit conservation equation provides the required haematocrit distribution (Bressloff et al., 2009).

The effect of the haematocrit distribution on the forcing in the z-direction is negligible and the forcing exhibits a parabolic distribution similar to the classic Poiseuille profile as that shown in Fig. (2). Moreover, the applied haematocrit forcing for the non-Newtonian case results in a change in the radial migration patterns as shown in Fig. (9). As mentioned before, with no haematocrit forcing, the WBC is seen to migrate towards the centreline at all radial locations. While with the addition of forcing based on haematocrit distribution, the WBC migration can be split into two regions. Below $r = 0.55$, the WBC still migrates towards the centreline, but at a reduced rate. Outside of this radial location, the WBC migrates towards the wall with an increased rate. This suggests that the WBC migration depends upon the initial radial location. An unstable equilibrium position exists at the critical location between the two regions. The same results are obtained for the radial velocity and illustrated in Fig. (10). These results concur with the findings of Freund (2007). WBCs likely tend to migrate towards the wall.

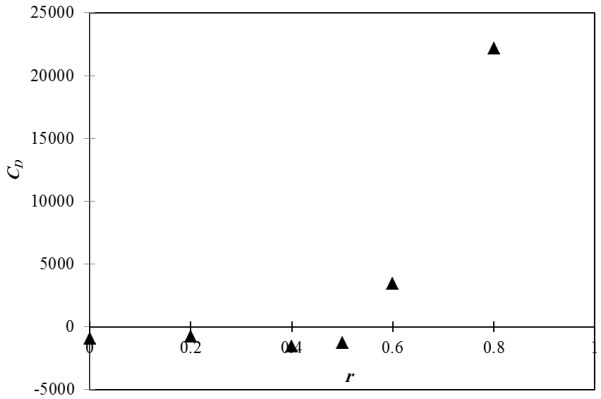

Fig. (9). Radial drag forcing coefficient with haematocrit forcing vs. radial location for the non-Newtonian case

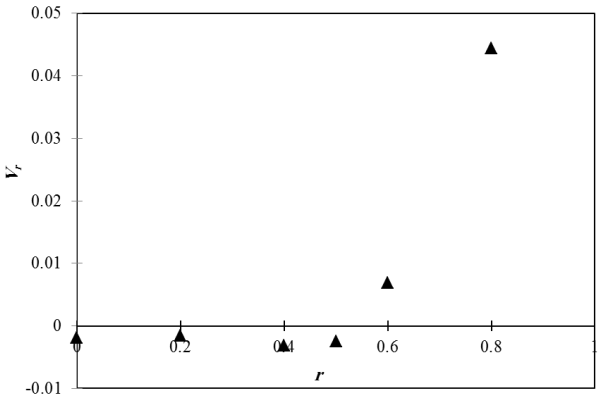

Fig. (10). Radial migration velocity with haematocrit forcing vs. radial location for the non-Newtonian case

5. Conclusions

A model has been developed to allow a white blood cell (WBC) to move through a microvessel using dynamic meshing and six-degree-of-freedom (SDOF) model. The

WBC motion is based on the pressure and shear forces on its surface. The haematocrit distribution is introduced to the model by using a new haematocrit scalar transport equation to take into account the effects of the haematocrit distribution on the WBC motion. The following conclusions are drawn:

- The WBC transitional velocity in the axial direction is lower than the fluid velocity for both the Newtonian and non-Newtonian flows.
- The slip velocity increases for the WBC flow in a non-Newtonian liquid than that in Newtonian liquid. Also, it increases as it releases closer to the wall.
- The WBC radial velocity magnitude is much lower than the transitional velocity magnitude and it always migrates to the centreline (does not depend on the initial WBC radial position).
- New correlations are developed for the particle axial and radial velocities for both Newtonian and non-Newtonian carrying fluids. This enables to estimate the WBC trajectories released at different locations.
- Haematocrit forces and the initial WBC radial position have a great effect on its equilibrium radial position. The WBC migrates towards the wall at normalized radial position r less than 0.55 and moves to the wall at r higher than 0.55. These results agree in some sense to the distribution of WBCs within a microvessel which exists in the literature (Freund, 2007). The main agreement is that near the wall the WBC is shown to migrate towards the wall, this matches the high probability of WBCs being located near the wall.

Nomenclature

Roman Characters

a Radius, m
C_D Drag coefficient
f Force, N
g Gravitational acceleration, m/s^2
H Haematocrit
K Consistency index for Power law model, Pa^n
l Arteriole length, m
L Inertia tensor, kg
m Mass, kg
M Moment vector, N.m
n Power or index for Power law model
p Pressure, N/m^2
r Normalized radial position (R/a_V)
R Radial position, m
RBC Red blood cell
Re Reynolds number
$\vec{S}$ Source term, kg/(m^{2}s^2)
t Time, s
u, v, w Velocity components, m/s
$\vec{V}$ Velocity vector, m/s
WBC White blood cell
x, y, z Cartesian position components, m

Greek Characters

β Dimensionless equilibrium position
Γ Diffusion coefficient, kg/(m^{2}s)
λ Particle to vessel radius ratio
μ Dynamic viscosity, Pa.s
ρ Density, kg/m^3
ρ' Density ratio
$\vec{\omega}$ Angular velocity vector, rad/s
$\dot{\vec{\omega}}$ Angular motion, m^2/s^2

Subscripts

B Blood
G Gravitational
M Mean
Max Maximum
r Component in a radial direction
S Relative velocity between WBC and undisturbed flow
T Translation
V Referring to Vessel
W Referring to WBC
x, y, z Component in specified Cartesian coordinates

References

[1] Alexandrova, A. & Antonova, N. 2012, Rheological and mechanical aspects of leukocytes motion and adhesion, *Series on Biomechanics*, **27** (3-4), 74-79.

[2] ANSYS FLUENT User's Guide: ANSYS Inc, 2010.

[3] Bressloff, N. W., Mansour, M. H., Shearman, C. P. 2009, Microvascular cell depletion model, *World Congress on Medical Physics and Biomedical Engineering, Munich, Germany*.

[3] Cox, R. G. & Mason, S. G. 1971, Suspended particles in fluid flow through tubes, *Annu. Rev. Fluid Mech.* **3**, 291-316.

[4] Fedosov, A. F., Fornleitner, J. & Gompper, G. 2012, Margination of white blood cells in microcapillary flow, *Phys. Rev. Letters 108 (2)*, 1-5.

[5] Feng, J., Hu H. H. & Joseph, D. D. 1994, Direct simulation of initial value problems for the motion of solid bodies in a Newtonian fluid. Part 2. Couette and Poiseuille flows, *J. Fluid Mech.* **277**, 271-301.

[6] Feng, Z.-G. & Michaelidis, E. E. 2002, Hydrodynamic force on spheres in cylindrical and prismatic enclosures, *International Journal of Multiphase Flow*, **28**, 479-496.

[7] Freund, J. B. 2007, Leukocyte margination in a model microvessel, *Physics of Fluids*, **19**, 1-12.

[8] Fung, Y. C. 1996, *Biomechanics: Circulation*, 2nd Edition, Springer, New York, USA.

[9] Karnis, A., Goldsmith, H. L. & Mason, S. G. 1966, The flow of suspensions through tubes. Part 5: Inertial effects. Can. J. Chem. Eng. 44, 181-193.

[10] Mahdi, A. S., Artoli, A. M. & Mathkour, H. I. 2014, Tracking leukocytes in vivo, *International Journal of Computer Science and Information Technologies*, **5** (1), 328-337.

[11] Matas, J. P., Morris, J. F. & Guazzelli, E. 2004, Lateral forces on a sphere, *Oil & Gas Science and Technology – Rev. IFP*, **59** (1), 60-70.

[12] Pan, T-W. & Glowinski, R. 2005, Direct simulation of the motion of neutrally buoyant balls in a three-dimensional Poiseuille flow, *C. R. Mécanique, Acad. Sci. Paris 333, 884-895*.

[13] Pozrikidis, C. 2005, Numerical simulation of cell motion in tube flow, *Annals of Biomedical Engineering*, **33** (2), 165-178.

[14] Segré, G. & Silberberg, A. 1961, Radial particle displacements in Poiseuille flow of suspensions, *Nature*, **189** (4760), 209-210.

[15] Schmid-Schönbein, G. W. *Rheology of Leukocytes*, in Skalak, R. & Chien, S. (Eds.) 1987, *Handbook of bioengineering*, McGraw-Hill Book Company, New York, USA.

[16] Shibeshi, S. & Collins, W. 2003. The rheology of blood flow in a branched arterial system, Appl. Rheol., 15, 398-405.

[17] Yang, H. B., Wang, J. Joseph, D. D., Hu, H. H., Pan, T.-W., & Glowinski, R. 2005, Migration of a sphere in tube flow, *J. Fluid Mech.*, **540**, 109-131.

[18] Yu, Z., Phan-Thien, N. & Tanner, R. I. 2004, Dynamic simulation of sphere motion in a vertical tube, *J. Fluid Mech.* **518**, 61-93.